Dynamic roughening of the magnetic flux landscape in $YBa_2Cu_3O_{7-x}$.

C. M. Aegerter [1] M. S. Welling R. J. Wijngaarden

Department of Physics and Astronomy; Vrije Universiteit; 1081HV Amsterdam; The Netherlands.

Abstract

We study the magnetic flux landscape in $YBa_2Cu_3O_{7-x}$ thin films as a two dimensional rough surface. The vortex density in the superconductor forms a self-affine structure in both space and time. This is characterized by a roughness exponent $\alpha = 0.76(3)$ and a growth exponent $\beta = 0.57(6)$. This is due to the structure and distribution of flux avalanches in the self-organized critical state, which is formed in the superconductor. We also discuss our results in the context of other roughening systems in the presence of quenched disorder.

Key words: PACS numbers:05.65.+b, 74.72.Bk, 64.60.Ht, 74.25.Qt

1 Introduction

When a type II superconductor is put in a slowly ramped external field, magnetic vortices start to penetrate the sample from its edges. These vortices get pinned by dislocations or other crystallographic defects, leading to the build-up of a flux gradient, which is only marginally stable, as is the slope of a slowly grown pile of sand [1]. Thus it can happen that small changes in the applied field can lead to large rearrangements of flux in the sample, known as flux avalanches [2]. Due to the analogy of the flux landscape with a pile of sand, the properties of flux avalanches have long been studied in the context of self-organized criticality (SOC) [3], which predicts that many slowly driven non-equilibrium systems have avalanches which are distributed according to a power-law [4]. As a matter of fact, vortex avalanches in superconductors are thought of as an ideal experimental system in which to study SOC, due

---

[1] Present address: Fachbereich Physik, Universität Konstanz, P.O. Box 5560, 78457 Konstanz, Germany.

to the over-damped dynamics of the vortices [2,5]. In the past, power-law distributed avalanches have been observed in many controlled experiments, which were ascribed to SOC [6]. Furthermore, the microscopic dynamics of the particles (vortices) is well known [7] and the collective dynamics can then be for instance studied in detail using molecular dynamics simulations [8]. In more detail however, SOC predicts that a system not only shows power-law behaviour, but that it organizes into a critical state, and should thus show finite-size scaling in the distribution of avalanches as well [9]. This has now also recently been shown for the flux-avalanches in a thin film of $YBa_2Cu_3O_{7-x}$ (YBCO) [10], where also the shape of the flux avalanches and their fractal dimension was characterised. The shape and distribution of avalanches moreover strongly influence the shape of the magnetic flux landscape, leading to a rough, self-affine surface [11]. The characteristic exponents of this surface can then be obtained quantitatively from the avalanche properties via a set of scaling relations derived by Paczuski *et al.* for many SOC models [12].

Here, we study the roughening properties of the magnetic flux landscape in a thin film of YBCO in two dimensions (2d). While dynamic roughening has been experimentally studied in many 1d systems [14,15,16], among which there was also a study of the front of penetrating flux in YBCO [17], 2d characterization of roughening systems are rare in the experimental literature [18]. A full 2d characterisation of the roughness properties makes it possible to compare properties of the avalanches with those of the surface, in order to have a stringent test for SOC in the flux avalanches in YBCO [10]. Furthermore, we compare the roughness results with numerical integrations of the Edwards-Wilkinson (EW) equation [13] in the presence of quenched disorder in order to have a comparison with the static pinning in the experiment.

Section 2 will describe the experimental setup in detail, while section 3 will introduce the analysis methods for a 2d surface, which are applied to the data. In section 4, we present the results of the numerical studies of the quenched EW equation, before turning to the roughness of the flux landscape in section 5. These roughness results will finally be compared with the avalanche properties, determined elsewhere [10], in section 6.

2   Experimental Setup

The magnetic flux density B_z just above the YBCO thin film is measured by means of the Faraday-effect [19] in an advanced magneto-optical microscope [20]. In this setup, the polarization rotation angle is measured directly by means of a lock-in technique. The YBCO films studied here were grown on a $NdGaO_3$ substrate to a thickness of 80 nm using pulsed laser ablation [21]. Pinning sites in the sample consist mostly of screw dislocations and are

distributed uniformly over the sample, acting as point pins [22].

The sample is cooled in zero applied field to 4.2 K, after which the field is slowly increased in steps of 50 μT, where at each field the sample is allowed to relax for 10 s before an image is taken with a high resolution charge coupled device camera (782×582 pixels) measuring the flux density $B_z(x, y)$. In each experiment, 300 such field steps are taken leading to a magnetic flux landscape as shown in Fig. 1. In the analysis, only the last 140 images of each run were used in order to have a flux landscape spanning more than 100 pixels. The results below come from a total of five such experiments on the same sample.
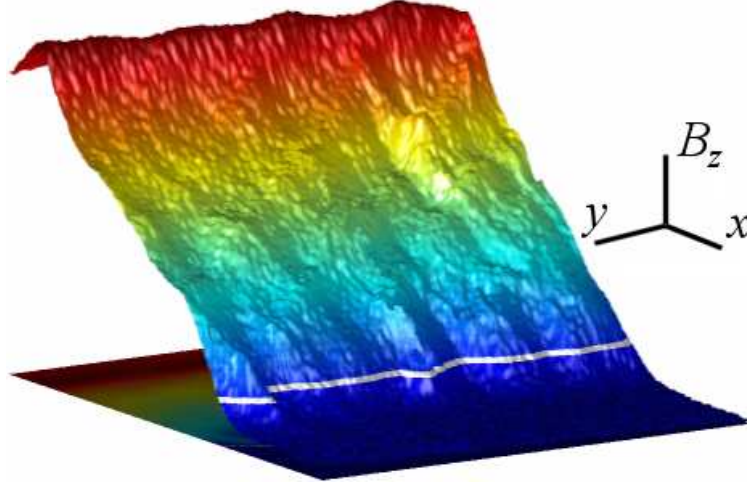

Fig. 1. The magnetic flux surface at an applied field of 12 mT in the YBCO thin film. As can be seen, when the flux density B_z is plotted as height, a shape reminiscent of a pile is obtained, which has a rough surface. The self-affine properties of the fluctuations around the mean surface are analysed below, after subtracting the average profile.

3 Analysis Methods

As can be seen from Fig. 1, the magnetic flux surface, $B_z(x, y)$, has an average profile, $\langle B_z(y) \rangle_x$, with high values near the sample edge and zero magnetic flux inside the sample, where $\langle \cdot \rangle_s$ denotes an average over the subscript s. In order to only study the properties of the fluctuations in the surface, this average profile is subtracted from the data, such that in the following the properties of $b(x, y) = B_z(x, y) - \langle B_z(y) \rangle_x$ are studied. Furthermore, the time evolution of the flux landscape is investigated by choosing the area which is studied to start at the mean position of the front of penetrating flux (indicated by the white line in Fig. 1) and going backwards towards the sample edge for 128 pixels. In this way a stationary state is mimicked where the height of the flux landscape is approximately constant in time. The level of the flux front

3

is chosen to be about three times the standard deviation of the noise in the Meissner phase, such that an accurate determination is possible.

The roughness of an interface is classically quantified via a determination of the width of the interface, as given by the second moment, $w(t, L)$ of the fluctuations around the mean interface [23]. For a roughening system characterized by a self-affine structure in space and time, the width increases with time as a power-law, $w(t) \propto t^\beta$, with the growth exponent β. At long times, after the correlation length has reached the system size, L, the width saturates at a value $w_{sat}(L) \propto L^\alpha$, depending on the system size again as a power-law [23]. Here, α is called the roughness exponent. In experiments, it is often more useful to determine the characteristic exponents from the correlation functions rather than from the interface width [24]. The correlation function, in 2d, is given by:

$$C^2(x, y, t) = \langle (h(\xi + x, \eta + y, \tau + t) - h(\xi, \eta, \tau))^2 \rangle_{\xi, \eta, \tau}. \tag{1}$$

In contrast to the width, the correlation function is obtained averaging over more points, leading to a more reliable estimate. The characteristic exponents can still be determined from the correlation function, since for a self-affine structure the scaling behaviour is as that of the width, i.e. $C(r, 0) \propto r^\alpha$ and $C(0, t) \propto t^\beta$ [23]. Here, $r = \sqrt{x^2 + y^2}$ is the radial distance in the plane.

Experimental noise in the apparatus (e.g. photon counting noise) may hamper the determination of the correlation function, such that power-law behaviour is lost at small scales. In our experiment, the flux surface $b(x, y)$ is in fact determined by contributions from both the ideal flux surface, $h(x, y)$ and experimental noise, predominantly due to photon counting noise, $\epsilon(x, y)$. Inserting a height fluctuation with an added noise component, $b(x, y) = h(x, y) + \epsilon(x, y)$ into the definition of the correlation function, one finds that the behaviour for the ideal fluctuations can still be obtained from the data, as long as the properties of the noise are known:

$$C_h^2(x, y, t) = C_b^2(x, y, t) - 2\sigma^2(x, y). \tag{2}$$

Here $\sigma(x, y)$ is the strength of the noise as given by $\langle \epsilon^2(x, y) \rangle$. In our system, we can experimentally determine the properties of the noise, such that a correction for the noise according to Eq. 2 and hence proper determination of the exponents is possible [25].

4

4 Numerical Simulations

In order to study the influence of quenched disorder, analogous to the static point pins in the superconductor, on the roughening properties of the flux surface, we also carried out numerical simulations of the two dimensional EW equation in the presence of static disorder. The EW equation describes the height of an interface, $h(x, y, t)$, as a function of time, which is pulled though a disordered medium with a speed v. In the experimental case, the driving can be seen as the increasing applied magnetic field H_{ext}. In this case, the
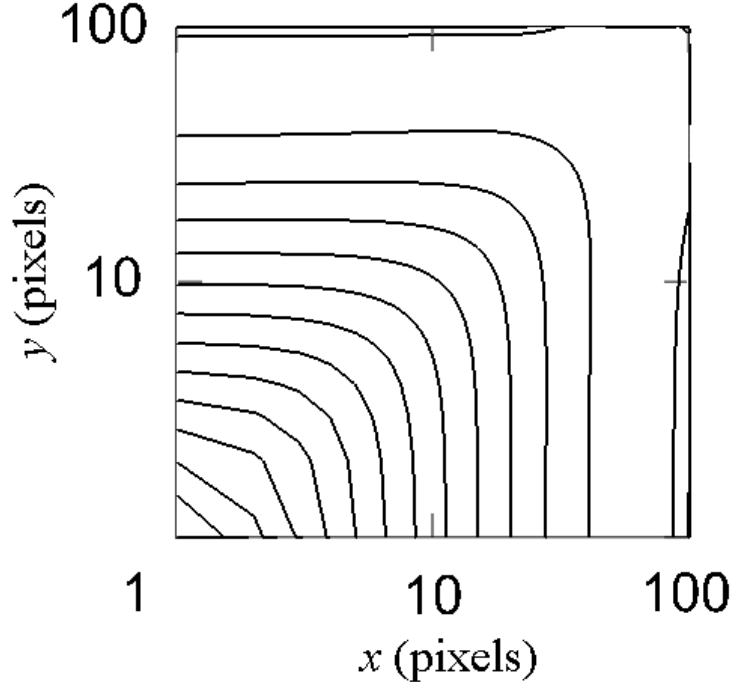

Fig. 2. Double logarithmic plot of the full 2d correlation function of the height fluctuations in the numerical simulation of the quenched EW equation. The contours are logarithmically spaced, such that equidistant contours indicate power-law behaviour. Furthermore, on a linear scale the contours are circular, indicating the isotropic nature of the system in the x- and y-directions (see also the inset of Fig. 3).

roughening of the interface is due to the disorder, $\eta(x, y, t)$, which is usually considered to have a white spectrum in both space and time. Furthermore, there is an elastic term, which leads to the smoothing of the surface [13].

$$\frac{\partial h(x, y, t)}{\partial t} = D \left(\left(\frac{\partial}{\partial x} \right)^2 + \left(\frac{\partial}{\partial y} \right)^2 \right) h(x, y, t) + \eta(x, y, t) + v. \qquad (3)$$

In the case of a white spectrum of the disorder, the equation can be solved exactly and in one dimension a self-affine interface is obtained, whereas in two

dimensions roughening is only marginal [23]. However, in the presence of a combination of quenched and dynamic disorder, the equation can no longer be solved analytically and numerical simulations show roughness also in 2d [26]. Here, we have numerically integrated the EW equation on a lattice of 128×128 pixels with periodic boundary conditions. In order to have both quenched and thermal disorder in the model, we add two disorder terms to the elastic term in Eq. 3, $\eta_q(x, y)$ and $\eta_d(x, y, t)$, where η_q is constant in time and represents the quenched part of the disorder and η_d has a white spectrum in time and represents the dynamic disorder. In the presence of quenched disorder we speak of the quenched EW equation. Both disorder terms have a white spectrum in space. The strength of both terms is equal for the results presented below, however the values of the exponents are very robust and ratios of $0.5 < \eta_q/\eta_d < 10$ yield the same exponents within errors. The integration is run for 10000 time steps until the width of the interface saturates and the full 2d correlation function is determined subsequently in 20 different simulations. In Fig. 2, the spatial component, $C(x, y)$, is shown in a logarithmic contour plot. Since the contours are logarithmically spaced, evenly spaced contours in the plot imply power-law behaviour. The fact that the contours are circularly shaped on a
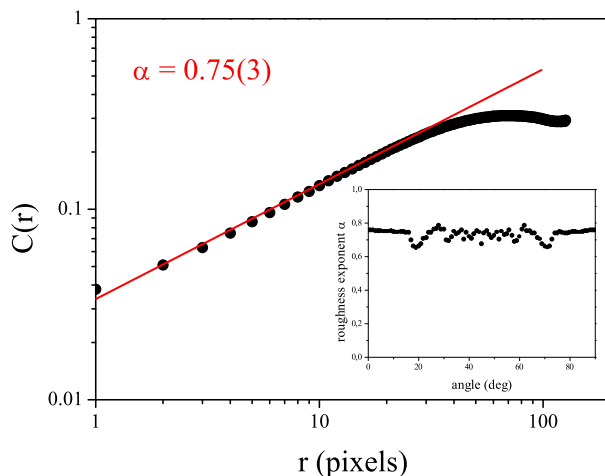

Fig. 3. Radial average of the full 2d correlation function of the height variations of the numerical simulation of the quenched EW equation. The straight line on the double logarithmic plot indicates power-law behaviour, where the slope of the curve determines the roughness exponent of $\alpha = 0.75(3)$. The inset shows the angular dependence of the roughness exponent α, as determined from a fit to different radial projections of the full 2d correlation function in the range of $r < 11$ pixels. The values of α are independent of the radial angle, as it should be for an isotropic system.

linear scale, indicates that the system is isotropic as it should be. This can also be seen by directly fitting a power-law dependence to radial projections of $C(x, y)$ over the range of $r < 11$ pixels. As can be seen in the inset to Fig. 3, the roughness exponent, α, does not depend on the radial angle, such that a

radial average, shown in the main part of the figure can be used to obtain a good determination of α. As can be seen, the correlation function is linear in the log-log plot over more than a decade with an exponent of $\alpha = 0.75(3)$, indicated by the straight line.
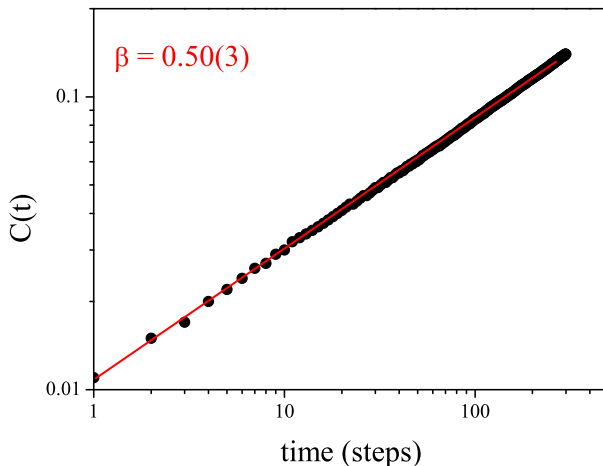

Fig. 4. The time correlation function for the numerical simulation of the quenched EW equation on a double logarithmic plot. The straight line indicates that the correlation function is a power-law with an exponent of $\beta = 0.50(3)$.

The temporal behaviour of the quenched EW equation can be characterized by the growth exponent β. This is determined from the temporal correlation function $C(t)$, which is shown in Fig. 4 on a double logarithmic scale. There is good power-law behaviour in the time correlation function, with a growth exponent of $\beta = 0.50(3)$, as determined from a linear fit over 100 time steps in the double logarithmic plot.

Thus in the presence of quenched disorder, the roughness properties of the EW equation change drastically with a strong increase of both the roughness and the growth exponent (in the absence of static disorder we obtain $\alpha \simeq \beta \simeq 0.1$). In the magnetic flux scape discussed below, the dynamics is mainly governed by the static pinning landscape, such that a model including quenched disorder is necessary in order describe the main features of the system. Note also that one of the standard sandpile models [27], which is used to describe the dynamics of a rice-pile, has been mapped exactly onto the quenched EW equation [28].

7

5 Flux landscape

Given the rough landscape shown in Fig. 1, we determine the self-affine properties of the fluctuations around the mean surface as discussed in Sec. 3 above. In order to have a reasonable size for the 2d area used in the analysis, we anal-
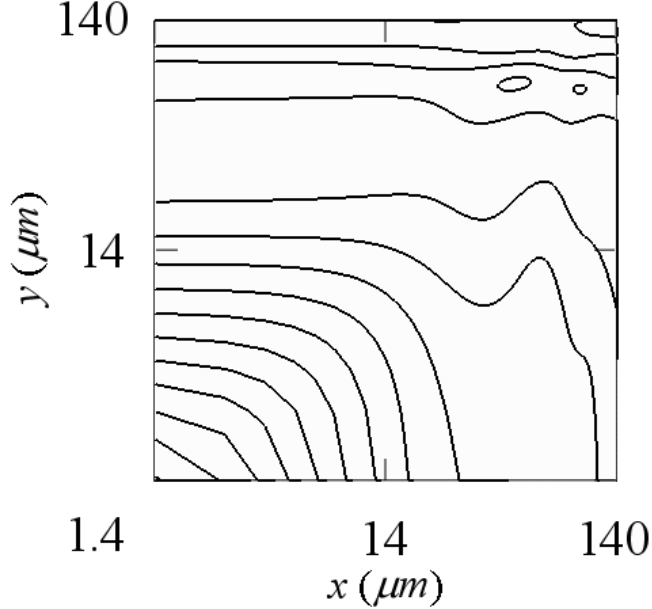

Fig. 5. Contour plot of the full 2d correlation function of the magnetic flux landscape. The contours are logarithmically spaced, such that equidistant contours imply a power-law dependence. The contours have a circular shape on a linear scale, which indicates that the system behaves isotropically in the x- and y-directions (see also inset of Fig. 6).

yse images starting from an applied field of 5 mT and determine the spatial and temporal correlation functions for the subsequent 128 images. Averaged over these 128 images and over all experiments, the full 2d correlation function, $C(x, y)$, is shown as a logarithmic contour plot in Fig. 5. As was the case in Fig. 2 above, the equidistant contours imply power-law behaviour and circular contours on a linear scale support the fact that the system is isotropic, such that a radial average may be performed in order to determine the roughness exponent more precisely. Another indication of of the isotropic nature of the system can be seen in the inset of Fig. 6, where the radial dependence of the roughness exponent is shown, as determined from a power-law fit on a scale $r < 35 \ \mu m$. As the figure shows, the roughness exponent does not depend on the radial angle, which means that a radial average can safely be carried out. The corresponding radial average, $C(r)$, is shown in the main part of Fig. 6, after a noise correction as described above [25], on a double logarithmic plot. As can be seen there is good power-law behaviour over more than one decade with a roughness exponent of $\alpha = 0.76(3)$, indicated by the straight line in
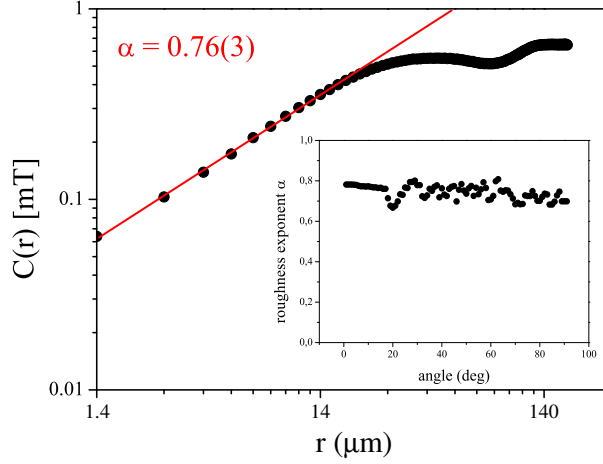
Fig. 6. Radial average of the correlation function of the magnetic flux surface. The inset shows the angular dependence of the roughness exponent α, as obtained from a power-law fit to the full 2d correlation function in the region $r < 35$ μm. The roughness exponent is independent of the radial angle, implying that the system is isotropic and that a radial average may be performed in order to determine α.

the figure. Again, the value of the exponent is obtained from a linear fit to the data in the double logarithmic plot in the range of $r < 35$ μm. The roughness exponent, which is obtained is in good agreement with that from the numerical integration of the quenched EW equation above.
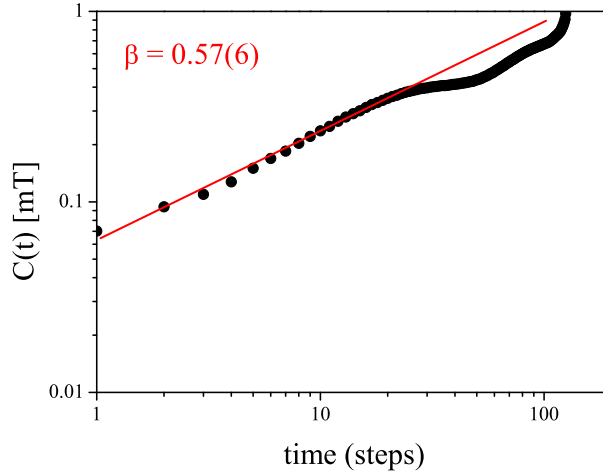

Fig. 7. The time correlation function for the magnetic flux surface. The straight line indicates power-law behaviour, with an exponent of $\beta = 0.57(6)$.

The temporal behaviour is characterized by the time correlation function of the height fluctuations. Again, noise in the experimental system distorts the data via an intrinsic width [25]. After correction for the experimentally determined noise, the data are plotted in Fig. 7. As can be seen, the correlation function

9

is a power-law over a decade in time, where the straight line in the figure indicates the exponent of $\beta = 0.57(6)$. Here, the exponent was obtained from a linear fit to the double logarithmic plot over the first 15 time steps. Again, this is in agreement with the result from the integration of the quenched EW equation. However, as mentioned above, the surface roughness is closely connected with the avalanche behaviour described by SOC [12]. The avalanche properties in our YBCO sample have been studied before, which allows a detailed quantitative comparison of the roughness properties with those of the avalanches [10]. This is done in the next section.

6   Comparison with Avalanche Properties

It has been noted that the roughness of a surface of a SOC system is created by the shape and distribution of the avalanches in the system [11]. Thus there should be a connection between these two phenomena, which can be tested [12]. Such a quantitative connection has been previously shown in the properties of the avalanches and the surface roughness of a three dimensional pile of rice [18]. From a theoretical point of view, the scaling relations have been derived in the context of models of extremal dynamics as well as the specific problem of a rice pile surface [12,18]. When the avalanches have a fractal dimension of D, which can be obtained from a finite-size scaling analysis of the avalanche size distribution and the active area of the avalanches has a fractal dimension of d_B, then the roughness exponent is given by $\alpha = D - d_B$. Using the values previously determined in the same YBCO samples [10] for the avalanche properties, i.e. $D = 1.89(3)$ and $d_B = 1.18(5)$, we obtain $\alpha = 0.71(6)$. This is in good agreement with the value of $\alpha = 0.76(3)$ determined above, as well as with the result from our numerical integration of the quenched EW equation. The growth exponent can be obtained via the dynamical exponent, $z = \alpha/\beta$, which describes the scale dependence of the cross-over time $t_\times$, at which the width of the surface saturates. This is given by $z = D(2 - \tau)$, where τ is the exponent of the avalanche size distribution. Again using the values from Ref. [10], $\tau = 1.29(2)$ and $D = 1.89(3)$, we obtain $z = 1.34(4)$ and hence $\beta = 0.53(9)$. This is in good agreement with the determination from the roughness analysis above, $\beta = 0.57(6)$, as well as with the results from the simulations of the quenched EW equation. Thus, not only can the Oslo-model [27] be mapped onto the quenched EW equation [28], also the more general scaling relations for SOC models derived by Paczuski *et al.* [12] can be checked in a system described by the quenched EW equation. This gives further support to the connection between SOC and roughening physics [29,30], which has already been shown for the surface of a pile of rice [18].

7 Conclusions

In conclusion, we have shown that the two dimensional flux surface of an YBCO thin film in the mixed state is self-affine and shows power-law scaling in its roughness and growth, given by $\alpha = 0.76(3)$ and $\beta = 0.57(6)$. Furthermore, this behaviour is in good agreement with the expectations from a simple roughening system (the EW equation) in the presence of quenched disorder. In addition, the surface roughness is connected to the avalanche properties of the magnetic flux jumps, as is expected for a SOC system. The scaling relations of Paczuski *et al.* [12], can be used to quantitatively predict the values of the roughness and growth exponents from the avalanche size distribution exponent and dimensions. Using an earlier characterisation of the avalanche properties in our sample [10], we obtain good agreement between the expectation from the scaling relations and the experimentally observed roughness exponents. This shows that the flux landscape in YBCO is formed by the avalanches of a SOC process. Also it shows the intimate connection between the roughening of an interface and avalanche dynamics, or SOC in general [29].

8 Acknowledgements

References

[1] P. G. de Gennes *Superconductivity of metals and alloys* (Addison-Wesley, 1966).

[2] A. M. Campbell, and J. E. Evetts, Adv. Phys. **21**, 199 (1972); reprinted *ibid* **50**, 1249 (2001); E. Altshuler and T. H. Johanson, Rev. Mod. Phys. to be published, cond-mat/040297 (2004).

[3] P. Bak, C. Tang, and K. Wiesenfeld, Phys. Rev. Lett. **59**, 381 (1987) and Phys. Rev. A **38**, 364 (1988).

[4] C. Tang, Physica A **194(1-4)**, 315 (1993); S. I. Zaitsev, Physica A **151**, 411 (1992).

[5] V. Frette, K. Christensen, A. Corral, J. Feder, T. Jøssang, Nature (London) **379**, 49 (1996).

[6] S. Field, J. Witt, and F. Nori, Phys. Rev. Lett. **74**, 1206 (1995); C. M. Aegerter, Phys. Rev. E **58**, 1438 (1998); K. Behnia, C. Capan, D. Mailly, and B. Etienne, Phys. Rev. B **61**, R3815 (2000); E. Altshuler, T. H. Johansen, Y. Paltiel, P. Jin, K. E. Bassler, O. Ramos, G. F. Reiter, E. Zeldov, and C. W. Chu, cond-mat/0208266.

[7] G. Blatter, M. V. Feigelman, V. B. Geshkenbein, A. I. Larkin, V. M. Vinokur, Rev. Mod. Phys. **66**, 1125 (1995).

[8] C. J. Olson, C. Reichhardt, and F. Nori, Phys. Rev. B **56**, 6175 (1997).

[9] H.-J. Jensen, *Self-organized criticality* (Cambridge Univ. Press., 2000).

[10] C. M. Aegerter, M. S. Welling, and R. J. Wijngaarden, Europhys. Lett. **65**, 573 (2004).

[11] Ch. Chen, M. den Nijs, Phys. Rev. E **66**, 011306 (2002).

[12] M. Paczuski, S. Maslov, and P. Bak, Phys. Rev. E **53**, 414 (1996); M. Paczuski, and S. Boettcher, Phys. Rev. Lett. **77**, 111 (1996).

[13] S. F. Edwards, and D. R. Wilkinson Proc. Roy. Soc. (London) **A381**, 17 (1982).

[14] E. Ben-Jacob, O. Shochet, A. Tenenbaum, I. Cohen, A. Czirók, and T.Vicsek, Nature(London) **368**, 46 (1994); S. Matsuura, and S. Miyazima, Fractals **1**, 336 (1993); T. Vicsek, M. Cserzö, and V. K. Horváth, Physica A **167**, 315 (1990).

[15] M. A. Rubio, C. A. Edwards, A. Dougherty, and J. P. Gollub, Phys. Rev. Lett. **63**, 1685 (1989); V. K. Horváth, F. Family, and T. Vicsek, J. Phys. A **24**, L25 (1991); S. He, G. L. M. K. S. Kahanda, and P.-Z. Wong, Phys. Rev. Lett. **69**, 3731 (1992).

[16] J. Maunuksela, M. Myllys, O. P. Kähkönen, J. Timonen, N. Provatas, M. J. Alava, and T. Ala-Nissila, Phys. Rev. Lett. **79**, 1515 (1997);A. Myllys, J. Maunuksela, A. Alava, T. Ala-Nissila, J. Merikoski, and J. Timonen, Phys. Rev. E **64**, 036101 (2001);J. Kertész, V. K. Horváth, and F. Weber, Fractals **1**, 67 (1993).

[17] R. Surdeanu, R. J. Wijngaarden, E. Visser, J. M. Huibrechtse, J. H. Rector, B. Dam, and R. Griessen, Phys. Rev. Lett. **83**, 2054 (1999).

[18] C. M. Aegerter, R. Günther, and R.J.Wijngaarden, Phys. Rev. E **67**, 051306 (2003).

[19] R. P. Huebener *Magnetic Flux Structures in Superconductors*, (Springer, 2nd ed. 2000); M. R. Koblischka, and R. J. Wijngaarden, Supercond. Sci. and Technol. **8**, 199 (1995).

[20] R. J. Wijngaarden, K. Heek, M. S. Welling, R. Limburg, and M. Pannetier, Rev. Sci. Instrum. **72**, 2661 (2001).

[21] B. Dam, J. Rector, M. F. Chang, S. Kars, D. G. de Groot, and R. Griessen, Appl. Phys. Lett. **65**, 1581 (1994).

[22] B. Dam, J. M. Huibrechtse, F. C. Klaassen, R. C. F. van der Geest, G. Doornbos, J. H. Rector, A. M. Tesla, S. Freisem, J. Aarts, J.-C. Martinez, B. Stäuble-Pümpin, and R. Griessen, Nature **399**, 439 (1999).

[23] see e.g. A. L. Barabasi and H. E. Stanley *Fractal Concepts in Surface Growth* (Cambridge University Press, 1995).

[24] J. Schmittbuhl, J.-P. Vilotte, and S. Roux, Phys. Rev. E **51**, 131 (1995); M. Siegert *ibid.* **53**, 3209 (1996); J. M. Lopez, M. A. Rodriguez, and R. Cuerno, *ibid.* **56**, 3993 (1997).

[25] M. S. Welling, C. M. Aegerter, and R. J. Wijngaarden, Europ. J. Phys. B in press (2004).

[26] T. Halpin-Healy, and Y.-C. Zhang, Phys. Rep. **254**, 215 (1995).

[27] K. Christensen, A. Corral, V. Frette, J. Feder, and T. Jøssang, Phys. Rev. Lett. **77**, 107 (1996).

[28] G. Pruessner, Phys. Rev. E **67**, 030301 (2003).

[29] M. Alava, and K. B. Lauritsen, Europhys. Lett. **53**, 569 (2001); G. Szabo, M. Alava, and J. Kertesz, Europhys. Lett. **57**, 665 (2002); M. Alava, J. Phys. C **14(9)**, 2353 (2002).

[30] A. Vespignani and S. Zapperi, Phys. Rev. Lett. **78**, 4793 (1997), Phys. Rev. E **57** 6345 (1998).